*31st EPS Conference on Plasma Phys. London, 28 June - 2 July 2004 ECA Vol.**28G**, P-5.172 (2004)*

'Complete' far-infrared polarimetry measurements at JET

K. Guenther and JET-EFDA contributors

EURATOM / UKAEA Fusion Association, Culham Science Centre, Abingdon, OX14 3DB, UK

1. Introduction

Far-infrared polarimetry is a well known tool to measure the poloidal field B_p in terms of the density-weighted line-of-sight integral of $B_{p\|}$ which is proportional to the Faraday rotation angle of the plane of polarization. This 'traditional' polarimetry provides important data to calculate the *q*-profile, but does not exploit the method completely: The output *ellipticity* of the beam, generated by the Cotton-Mouton effect (birefringence of a magnetized plasma), carries line-integrated information on density n_e times field components perpendicular to the direction of the beam. This concerns – in good approximation – the toroidal field B_t *alone*, which is, *in the case of vertical chords*, largely constant along the line of sight. Hence, *complete polarimetry* can additionally deliver the line-integrated density [1], which is otherwise measured routinely by interferometry with the drawback of fringe jumps [2].

It is the phase shift Φ' between the wave components parallel and perpendicular to B_t which is proportional to $\int n_e dz$ (vertical chord!). Its measurement requires the input polarization to be *different* from parallel or perpendicular ($\Theta' = 0$ or 90°), contrary to the customary approach. The latter aims to *suppress* the Cotton-Mouton effect as much as possible in order to obtain the rotation angle in a most simple way and get round the obstacle of spurious ellipticity generated in the optical system. *Complete* polarimetry, however, needs to tackle this serious problem, and the way it has been solved at JET is a major topic of this paper.

Another issue where novel results are presented is the *mutual interference of Faraday and Cotton-Mouton effects*: The former changes the phase shift, too, and the latter has an impact on the polarization angle. The pertinent theory that allows approximate reconstruction of the 'pure' effects is given in [3]; its crucial test on experimental data is subject of Section 5.

2. Experimental set-up

The instrument at JET comprises four vertical and four lateral channels (chords) with the same probing beams utilized for interferometry as well. The schematic in Fig. 1

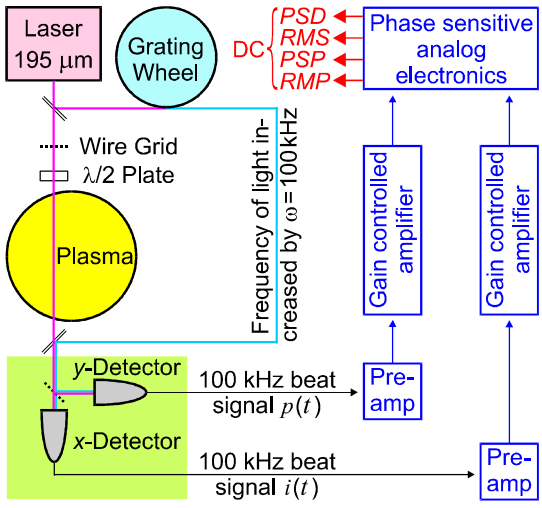

Fig. 1. Polarimetry set-up at JET. The half-wave plate at the entrance window is used to set the required direction of the *linear input polarization* and, by being rotated, provides a *calibration measurement* before each discharge. The amplitudes of the beat signals are proportional to the corresponding electric field vector amplitudes of the electromagnetic wave in the local co-ordinate system defined by the orientation of the wire grid in front of the detectors:

$$i(t) \propto E_x^{(0)} \cos(\omega t) \quad \text{and} \quad p(t) \propto E_y^{(0)} \cos(\omega t - \varphi)\,.$$

The electronics evaluates these signals by analog multiplication and integration (2, 5, 10 ms settable) according to

$$PSD = \langle p(t) \times i(t) \rangle \qquad RMS = \langle i(t) \times i(t) \rangle$$
$$PSP = \langle p(t) \times i'(t) \rangle \qquad RMP = \langle i'(t) \times i'(t) \rangle$$

where $i'(t) \propto E_x^{(0)} \sin(\omega t)$ is generated by phase shifting $i(t)$.

shows the essential experimental details for one channel. The four DC output signals, recorded with 14ms resolution, are processed numerically to produce the following basic signals:

$$R = PSD/RMS = C^{-1}\tan\Theta\cos\varphi \qquad R' = PSP/\sqrt{RMS\cdot RMP} = C^{-1}\tan\Theta\sin\varphi, \quad (1)$$

where the amplitude ratio angle Θ is defined by $\tan\Theta = E_y^{(0)}/E_x^{(0)}$ and the phase shift angle φ includes a constant offset ϕ_0 due to grated-beam ellipticity, electronics, etc.: $\varphi = \Phi + \phi_0$.

In the calibration measurement with *linearly* polarized light ($\lambda/2$ plate!), i.e. $\Phi = 0$, φ should be constant and the varied input polarization angle Θ' should figure in Eqs (1) save for an unknown offset: $\Theta = \Theta' + \Theta_0$. Thus, it should be straightforward to find the three calibration parameters ϕ_0, Θ_0, and C. Not so in reality! φ varies along with Θ' as the experimental functions $R(\Theta')$ and $R'(\Theta')$ have no common zeros, indicating *spurious ellipticity*.

3. A model to account for and eliminate spurious ellipticity

There are several ways to try and explain the origin of spurious ellipticity. Some were put to the test quantitatively (accuracy of fit of calibration data) and had to be rejected, including the assumption of an imperfect half-wave plate. The one that works consists in a model which assumes that an optical element (window, recombination plate?) generates a *constant* phase shift $\tilde{\phi}$ that refers to a *rotated* co-ordinate system of unknown orientation Ξ.

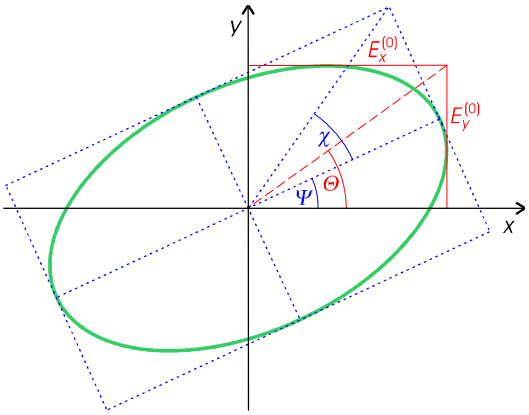

Fig. 2. Definition of parameters that describe the polarization state of elliptically polarized light.

Figure 2 shows the geometrical parameters Ψ and χ (polarization angle Ψ and ellipticity $\varepsilon = \tan\chi$) which describe the polarization state of light as completely as the characteristics of the electric field vector, i.e. amplitude ratio $\tan\Theta$ and phase shift angle Φ. The transformation between these two representations is given by (see [3], [4])

$$\cos2\Theta = \cos2\chi\cos2\Psi \quad (2)$$

$$\tan\Phi = \tan2\chi/\sin2\Psi \quad (3)$$

$$\tan2\Psi = \tan2\Theta\cos\Phi \quad (4)$$

$$\sin2\chi = \sin2\Theta\sin\Phi\ . \quad (5)$$

These relations, valid in any co-ordinate system, are essential to evaluate the model as shown

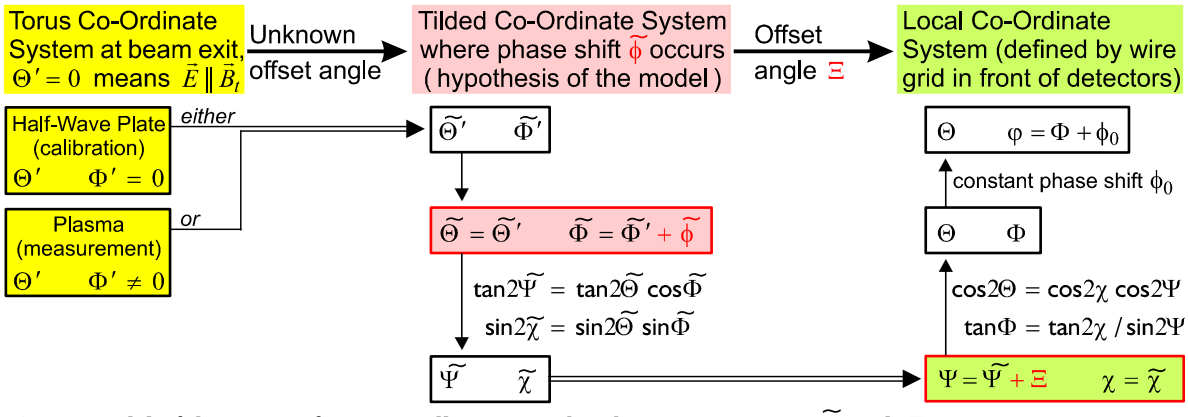

Fig. 3. Model of the origin of spurious ellipticity with unknown parameters $\tilde{\phi}$ and Ξ.

in Fig. 3. Although the model has *two* unknown parameters, its evaluation yields only *one*,

$$\sin2\xi = \sin2\Xi\sin\tilde{\phi}\ , \quad (6)$$

apart from two other new parameters, ϕ and Θ_0', which, however, incorporate the old ones,

ϕ_0 and Θ_0, favourably: $\phi = \widetilde{\Phi}_0 + \phi_0$ and $\Theta'_0 = \widetilde{\Theta}_0 + \Xi - \Theta_0$, where $\tan\widetilde{\Phi}_0 = \cos 2\Xi \tan\widetilde{\phi}$ and $\tan 2\widetilde{\Theta}_0 = -\tan 2\Xi \cos\widetilde{\phi}$. The final result as far as calibration is concerned ($\widetilde{\Phi}' = 0$) reads

$$\mathbf{R} = \begin{pmatrix} R \\ R' \end{pmatrix} = C^{-1}\mathbf{M}\cdot\begin{pmatrix} \sin 2\Theta^* / (1+\cos 2\xi \cos 2\Theta^*) \\ \sin 2\xi \cos 2\Theta^* / (1+\cos 2\xi \cos 2\Theta^*) \end{pmatrix} \qquad \mathbf{M} = \begin{pmatrix} \cos\phi & \sin\phi \\ \sin\phi & -\cos\phi \end{pmatrix}, \quad (7)$$

where $\Theta^* = \Theta' - \Theta'_0$. These relations can be combined in such a way that *linear* least-squares fits concerning the four calibration parameters are possible. The latter then serve to evaluate the plasma measurement in terms of $\Delta\Psi$ and χ. Rather lengthy algebra (Fig. 3 with $\widetilde{\Phi}' \neq 0$) yields

$$\Delta\Psi = \left[\operatorname{atan2}(r_1, F\cos 2\xi + r_2 \sin 2\xi) - 2\Theta^*(0)\right] / 2 \qquad \sin 2\chi = F\sin 2\xi - r_2 \cos 2\xi \quad (8)$$

$$\mathbf{r} = 2\mathbf{r}_{\text{aux}} / (1+\mathbf{r}_{\text{aux}}^2) \qquad F = (1-\mathbf{r}_{\text{aux}}^2)/(1+\mathbf{r}_{\text{aux}}^2) \qquad \mathbf{r}_{\text{aux}} = C\,\mathbf{M}\cdot\mathbf{R} \qquad \sin 2\Theta^*(0) = r_1(0) .$$

Quantities like $r_1(0)$ are baseline quantities referring to the situation before the discharge. So, $\Psi'_0 = \Theta'(0) = \Theta^*(0) + \Theta'_0$ is the initial polarization angle in the torus co-ordinate system in which the phase shift has to be calculated: $\tan\Phi' = \tan 2\chi' / \sin 2\Psi' = \tan 2\chi / \sin 2(\Delta\Psi + \Psi'_0)$.

4. Some experimental results

A calibration measurement typical of large spurious ellipticity and its evaluation in terms of Eq (7) is shown in Fig. 4. The excellent fit of φ lends probability to the model, while the slight deviations of R and R' at large angles can be attributed to non-linearities of the electronics and handled accordingly (non-constant C) by means of a fifth calibration parameter.

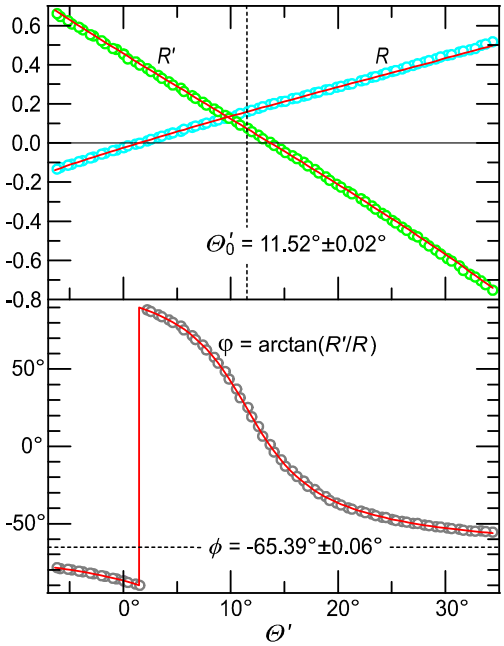

Fig. 4. Calibration data (Ch. 6) fitted according to Eq (7): $\xi = -4.83° \pm .01°$, $C = 0.482 \pm .001$.

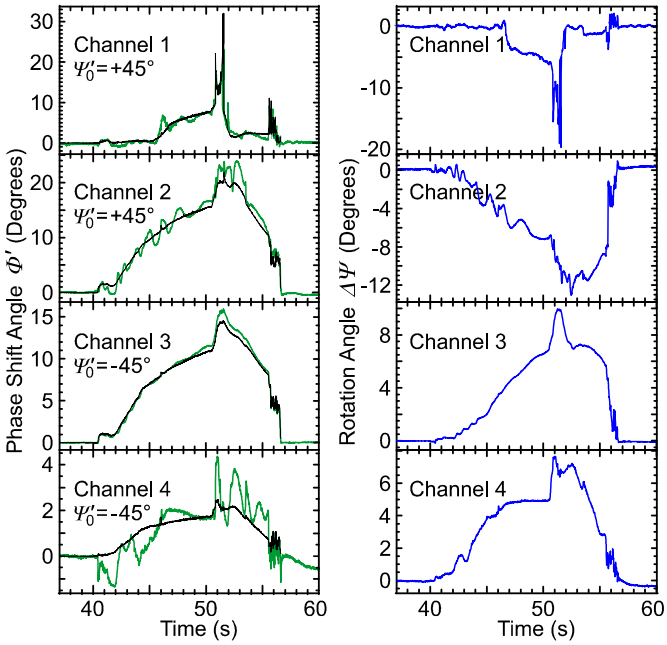

Fig. 5. JET Pulse 62981 ($B_t = 3.4$ T, $I_p = 2$ MA), results of polarimetry on vertical chords (radii/m: 1.890, 2.702, 3.040, 3.738).

A complete vertical-system measurement is presented in Fig. 5. The black lines show the interferometric $\int n_e \mathrm{d}z$ expressed as a Cotton-Mouton phase shift angle according to [3]

$$\Phi' = \int \left(eB_t/m_e\right)^2 \omega_{\text{plasma}}^2 \Big/ \left(2c\omega_{\text{light}}^3\right) \mathrm{d}z = 2.4568\times 10^{-11} \left(\lambda/\mathrm{m}\right)^3 \left(B_t/\mathrm{T}\right)^2 \int n_e \,\mathrm{d}z / \mathrm{m}^{-2} . \quad (9)$$

The agreement is remarkable. The interaction of the two effects (Section 5) is unimportant in this case. The origin of the very detrimental spurious oscillations of the signals has not yet been clearly identified; they must be down to oscillations of optical components (cf. [5]).

5. Mutual interference of Faraday effect and Cotton-Mouton effect

This phenomenon, though theoretically evident [3] and well known, has so far been disregarded in practice. Rightly so for small plasmas and the standard set-up $\Psi_0' = \Theta'(0) = 0$. High-density plasmas in the large JET device, however, can produce rotation angles and phase shift angles which have little to do with the Faraday and Cotton-Mouton ones, respectively. This can be demonstrated by comparing polarimetry results obtained on very *similar*

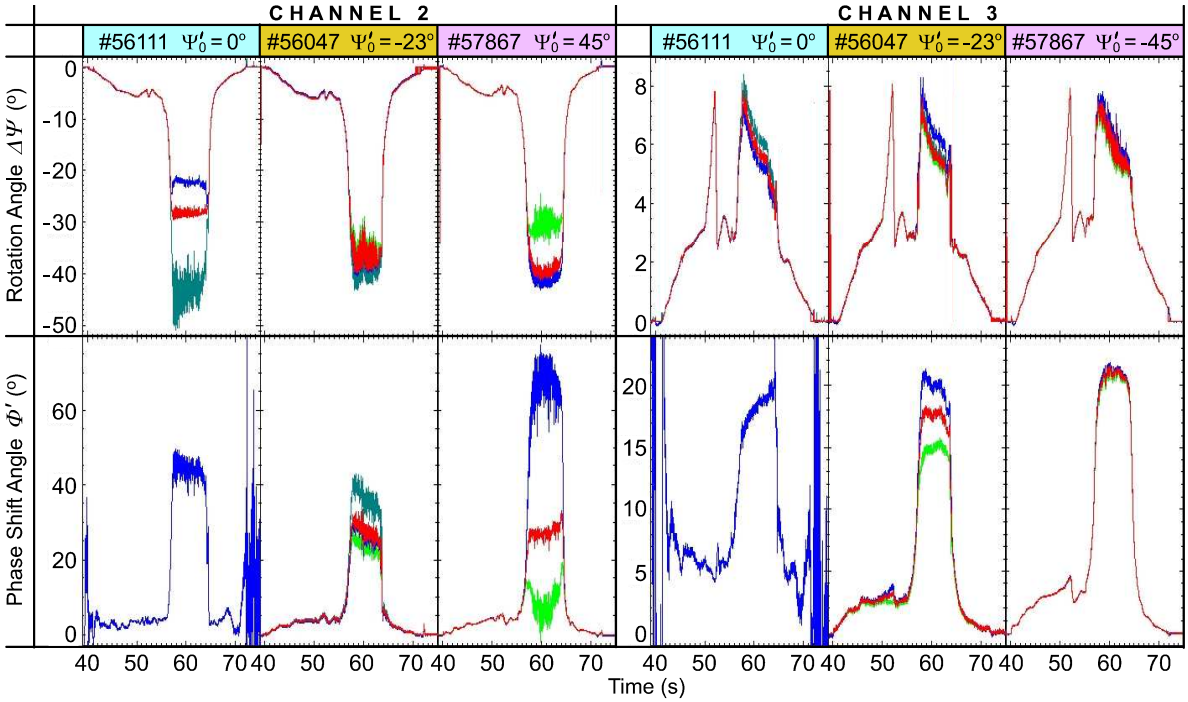

Fig. 6. Results from similar shots ($B_t = 2.7$ T, $I_p = 2.5$ MA): Blue traces as measured. Red lines show the so-called 'model mean values', green lines the limits, both calculated, according to [3], from the experimental data.

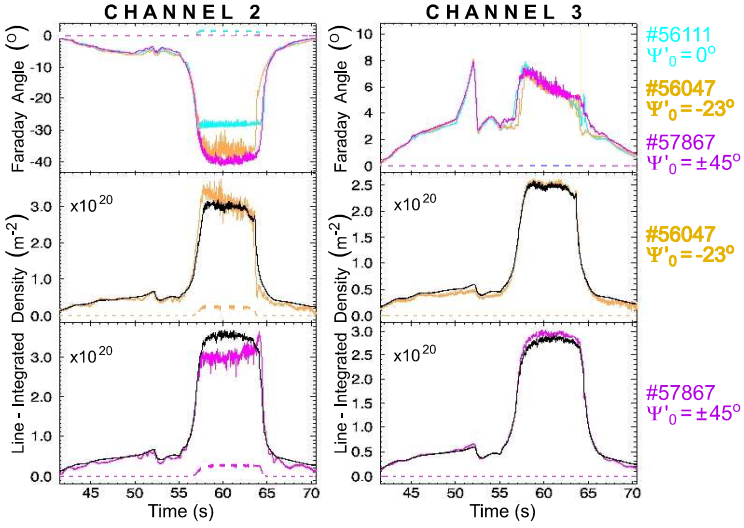

Fig. 7. Comparison of 'model means' and their uncertainties (dotted).

discharges, using *different* Ψ_0's. Fig. 6 shows a suitable triplet of shots with the red lines to demonstrate the capability of the method [3] to recover the 'pure' quantities expected to be broadly equal.

The latter alone are re-plotted in Fig. 7 to visualize the equality – except for Channel 2 of #56111 – of the pure Faraday angles and the relevance of the Cotton-Mouton angles expressed as line-integrated densities according to Eq (9) – black lines show the interferometric $\int n_e \mathrm{d}z$.

Work performed under the European Fusion Development Agreement (EFDA) and partly funded by the United Kingdom Engineering and Physical Sciences Research Council and by EURATOM.

[1] S.E. SEGRE, Plasma Phys. Control. Fusion **35** (1993) 1261.
[2] L. ZABEO et al., 30th EPS Conf. on Contr. Fusion and Plasma Phys., 2003, P-4.82.
[3] K. GUENTHER, Plasma Phys. Control. Fusion, *in print.*
[4] M. BORN and E. WOLF, *Priciples of Optics*, Oxford, Pergamon, 1964.
[5] D. ELBÈZE et al., 30th EPS Conf. on Contr. Fusion and Plasma Phys., 2003, P-4.79.